Vol 466|22 July 2010|doi:10.1038/nature09211

LETTERS

Atomically precise bottom-up fabrication of graphene nanoribbons

Jinming Cai[1]*, Pascal Ruffieux[1]*, Rached Jaafar[1], Marco Bieri[1], Thomas Braun[1], Stephan Blankenburg[1], Matthias Muoth[2], Ari P. Seitsonen[3,4], Moussa Saleh[5], Xinliang Feng[5], Klaus Müllen[5] & Roman Fasel[1,6]

Graphene nanoribbons—narrow and straight-edged stripes of graphene, or single-layer graphite—are predicted to exhibit electronic properties that make them attractive for the fabrication of nanoscale electronic devices[1–3]. In particular, although the two-dimensional parent material graphene[4,5] exhibits semimetallic behaviour, quantum confinement and edge effects[2,6] should render all graphene nanoribbons with widths smaller than 10 nm semiconducting. But exploring the potential of graphene nanoribbons is hampered by their limited availability: although they have been made using chemical[7–9], sonochemical[10] and lithographic[11,12] methods as well as through the unzipping of carbon nanotubes[13–16], the reliable production of graphene nanoribbons smaller than 10 nm with chemical precision remains a significant challenge. Here we report a simple method for the production of atomically precise graphene nanoribbons of different topologies and widths, which uses surface-assisted coupling[17,18] of molecular precursors into linear polyphenylenes and their subsequent cyclodehydrogenation[19,20]. The topology, width and edge periphery of the graphene nanoribbon products are defined by the structure of the precursor monomers, which can be designed to give access to a wide range of different graphene nanoribbons. We expect that our bottom-up approach to the atomically precise fabrication of graphene nanoribbons will finally enable detailed experimental investigations of the properties of this exciting class of materials. It should even provide a route to graphene nanoribbon structures with engineered chemical and electronic properties, including the theoretically predicted intraribbon quantum dots[21], superlattice structures[22] and magnetic devices based on specific graphene nanoribbon edge states[3].

Figure 1 sketches the basic graphene nanoribbon (GNR) fabrication steps for the prototypical armchair ribbon[6] of width $N = 7$ obtained from 10,10′-dibromo-9,9′-bianthryl precursor monomers. Thermal sublimation of the monomers onto a solid surface removes their halogen substituents, yielding the molecular building blocks of the targeted graphene ribbon in the form of surface-stabilized biradical species. During a first thermal activation step, the biradical species diffuse across the surface and undergo radical addition reactions[17] to form linear polymer chains as imprinted by the specific chemical functionality pattern of the monomers. In a second thermal activation step a surface-assisted cyclodehydrogenation establishes an extended fully aromatic system.

Figure 2 shows GNRs obtained according to the scheme in Fig. 1, using precursor monomers **1** and a Au(111) surface. The first step to GNR fabrication—intermolecular colligation through radical addition—is thermally activated by annealing at 200 °C, at which temperature the dehalogenated intermediates have enough thermal energy to diffuse along the surface and form single covalent C–C bonds between each monomer to give polymer chains. Scanning tunnelling microscopy (STM) images of the colligated monomers show protrusions that appear alternately on both sides of the chain axis and with a periodicity of 0.86 nm (Fig. 2b), in excellent agreement with the periodicity of the bianthryl core of 0.85 nm. Steric hindrance between the hydrogen atoms of adjacent anthracene units rotates the latter around the σ-bonds connecting them, resulting in opposite tilts of successive anthracene units with respect to the metal surface. This deviation from planarity explains the large apparent height of the polyanthrylenes of about 0.4 nm (Fig. 2b), with the finite size of the scanning probe tip moreover imaging the polymer with a width much larger (1.5 nm) than expected from the structural

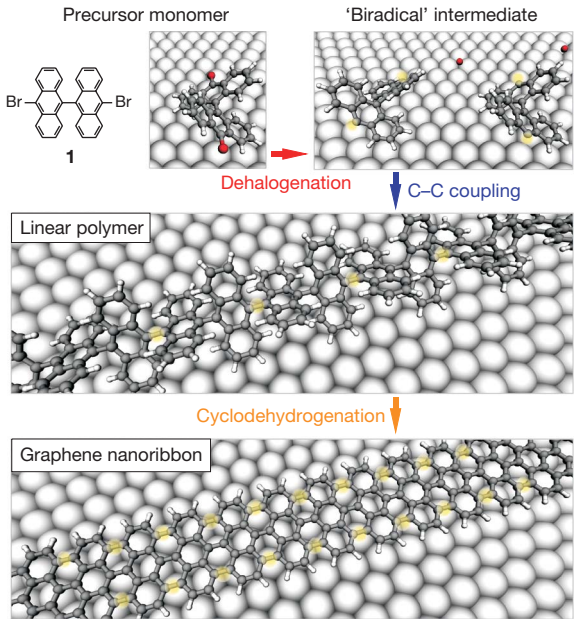

Figure 1 | Bottom-up fabrication of atomically precise GNRs. Basic steps for surface-supported GNR synthesis, illustrated with a ball-and-stick model of the example of 10,10′-dibromo-9,9′-bianthryl monomers (**1**). Grey, carbon; white, hydrogen; red, halogens; underlying surface atoms shown by large spheres. Top, dehalogenation during adsorption of the di-halogen functionalized precursor monomers. Middle, formation of linear polymers by covalent interlinking of the dehalogenated intermediates. Bottom, formation of fully aromatic GNRs by cyclodehydrogenation.

[1]Empa, Swiss Federal Laboratories for Materials Science and Technology, nanotech@surfaces Laboratory, 3602 Thun and 8600 Dübendorf, Switzerland. [2]ETH Zurich, Department of Mechanical and Process Engineering, Micro and Nanosystems, 8092 Zurich, Switzerland. [3]University of Zurich, Physical Chemistry Institute, Winterthurerstrasse 190, 8057 Zurich, Switzerland. [4]IMPMC, CNRS and Université Pierre et Marie Curie, 4 place Jussieu, case 115, F-75252 Paris, France. [5]Max Planck Institute for Polymer Research, Ackermannweg 10, 55124 Mainz, Germany. [6]Department of Chemistry and Biochemistry, University of Bern, Freiestrasse 3, 3012 Bern, Switzerland.
*These authors contributed equally to this work.

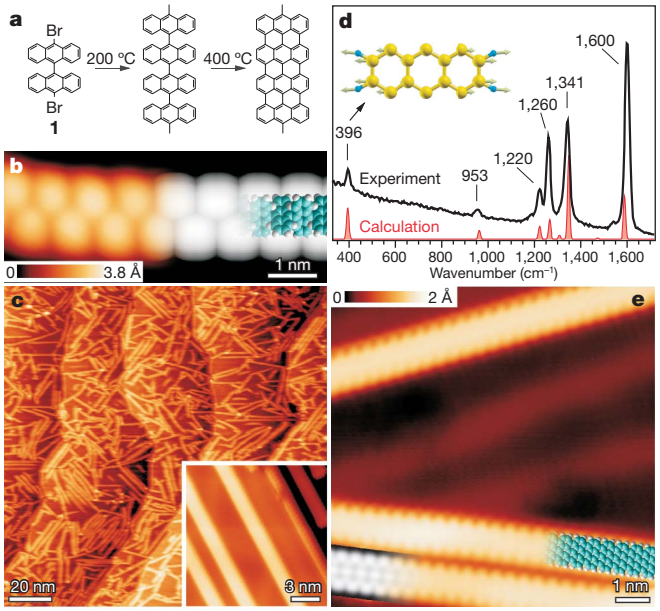

Figure 2 | Straight GNRs from bianthryl monomers. **a**, Reaction scheme from precursor **1** to straight $N = 7$ GNRs. **b**, STM image taken after surface-assisted C–C coupling at 200 °C but before the final cyclodehydrogenation step, showing a polyanthrylene chain (left, temperature $T = 5$ K, voltage $U = 1.9$ V, current $I = 0.08$ nA), and DFT-based simulation of the STM image (right) with partially overlaid model of the polymer (blue, carbon; white, hydrogen). **c**, Overview STM image after cyclodehydrogenation at 400 °C, showing straight $N = 7$ GNRs ($T = 300$ K, $U = -3$ V, $I = 0.03$ nA). The inset shows a higher-resolution STM image taken at 35 K ($U = -1.5$ V, $I = 0.5$ nA). **d**, Raman spectrum (532 nm) of straight $N = 7$ GNRs. The peak at 396 cm^{-1} is characteristic for the 0.74 nm width of the $N = 7$ ribbons. The inset shows the atomic displacements characteristic for the radial-breathing-like mode at 396 cm^{-1}. **e**, High-resolution STM image with partly overlaid molecular model (blue) of the ribbon ($T = 5$ K, $U = -0.1$ V, $I = 0.2$ nA). At the bottom left is a DFT-based STM simulation of the $N = 7$ ribbon shown as a greyscale image.

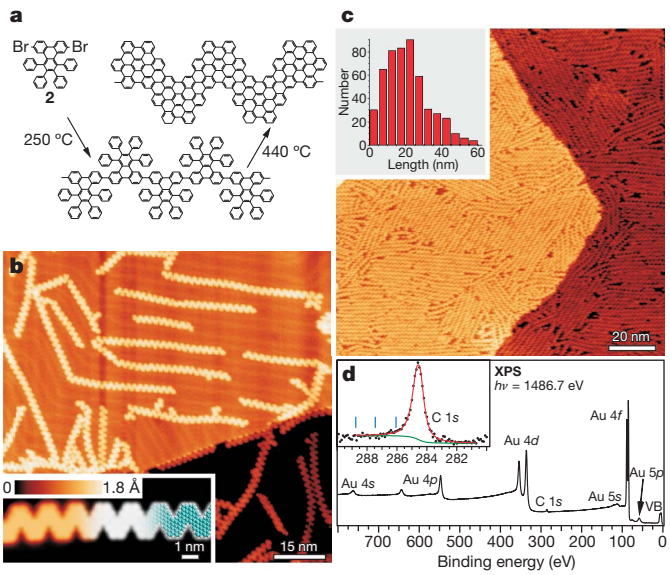

Figure 3 | Chevron-type GNRs from tetraphenyl-triphenylene monomers. **a**, Reaction scheme from 6,11-dibromo-1,2,3,4-tetraphenyltriphenylene monomer **2** to chevron-type GNRs. **b**, Overview STM image of chevron-type GNRs fabricated on a Au(111) surface ($T = 35$ K, $U = -2$ V, $I = 0.02$ nA). The inset shows a high-resolution STM image ($T = 77$ K, $U = -2$ V, $I = 0.5$ nA) and a DFT-based simulation of the STM image (greyscale) with partly overlaid molecular model of the ribbon (blue, carbon; white, hydrogen). **c**, Monolayer sample of chevron GNRs on Au(111): STM image and corresponding ribbon length distribution. **d**, XPS survey of a monolayer sample of chevron-type GNRs with core levels and valence band (VB) labelled. The C1s core level spectrum (inset) consists of a single component located at 284.5 eV binding energy (full-width at half-maximum, FWHM 0.87 eV). The absence of oxygen-related spectral features proves the chemical inertness of the GNRs with respect to ambient conditions: blue bars indicate the energy position for C–O, C = O and COOH (with increasing chemical shift); see text.

model (1.0 nm). STM simulations (Fig. 2b, right side, greyscale) that account for the finite tip radius perfectly reproduce the apparent height and width of the polyanthrylenes. The fully aromatic system is obtained by annealing the sample in a second step at 400 °C, which induces intramolecular cyclodehydrogenation of the polymer chain and hence the formation of an $N = 7$ armchair ribbon (Fig. 2c) with half the periodicity of the polymeric chain (0.42 nm) and a markedly reduced apparent height of 0.18 nm (Supplementary Fig. 3). STM simulations are in perfect agreement with experimental images (Fig. 2e), confirming that the reaction products are atomically precise $N = 7$ GNRs with fully hydrogen-terminated armchair edges.

The Raman spectrum in Fig. 2d of a densely packed layer of $N = 7$ armchair GNRs grown on a 200-nm Au(111) film on a mica substrate further attests to the uniform width of the ribbons: besides the D and G peaks[23] and several other peaks appearing due to the finite width and low symmetry of the ribbons, the spectrum exhibits the width-specific radial-breathing-like mode[24] as a sharp peak at 396 cm^{-1} (in excellent agreement with our calculated value of 394 cm^{-1}). This implies that the radial-breathing-like mode is indeed a sensitive probe of GNR width ($N = 6$ and $N = 8$ GNRs have radial-breathing-like mode frequencies about 50 cm^{-1} higher and lower, respectively[24]).

In our method the topology of the GNRs produced is determined by the functionality pattern of the precursor monomers, allowing the fabrication of ribbons with complex shapes. As an example, Fig. 3a illustrates the strategy for fabricating chevron-type GNRs with alternating widths of $N = 6$ and $N = 9$ using 6,11-dibromo-1,2,3,4-tetraphenyltriphenylene precursor monomers **2**. Initial colligation of the dehalogenated intermediates on Au(111) at 250 °C yields chains, in which adjacent monomers have opposite orientation with respect to the polymer main axis (Supplementary Fig. 2). The fully aromatic GNR is then produced during a second annealing step at 440 °C, which causes intramolecular cyclodehydrogenation of the polymer chain as is shown by a reduction of the apparent height from 0.25 nm to 0.18 nm (Supplementary Fig. 3). The resultant chevron-type GNRs have a periodicity of 1.70 nm and a pure armchair edge structure (Fig. 3b, c). Comparisons with the model structure and with density function theory (DFT) -based STM simulations (Fig. 3b) confirm that the structure of the chevron-type ribbon has been imposed by the colligated and cyclodehydrogenated monomer **2**.

Figure 3c shows a monolayer thin film of $N = 6/N = 9$ chevron-type armchair GNRs, with the degree of alignment between neighbouring GNRs improved over that seen in low-coverage samples. The preferred growth direction of the GNRs is given by the herringbone reconstruction of the Au(111) substrate. The substrate-controlled growth direction also limits the ribbon length: The length histogram (inset in Fig. 3c) drops significantly above ~30 nm, which corresponds to the typical length of the straight segments of the herringbone reconstruction of the Au(111) sample used. A significant increase in ribbon length can thus be expected for template surfaces favouring unidirectional ribbon growth[25,26].

An X-ray photoelectron spectroscopy (XPS) analysis of a monolayer thin film of $N = 6/N = 9$ chevron-type armchair GNRs grown on a Au(111)/mica surface was performed after sample transfer through air and subsequent annealing to 450 °C under ultrahigh-vacuum conditions to desorb volatile contaminants accumulated during air exposure. The overview XPS spectrum shown in Fig. 3d exhibits only core level peaks owing to the gold substrate and the GNRs. The enlarged view of the C1s core level region in the inset shows that the C 1*s* peak consists of a single sharp component at

284.5 eV binding energy characteristic of sp^2 bonded carbon. There are no signs of carbon in other chemical environments, and in particular no C–O, C=O or COOH components[27]. We conclude that the GNRs are chemically pure, and inert under ambient conditions. XPS also shows that the halogens desorb from the surface before the final cyclodehydrogenation step.

Suitably designed halogen-functionalized molecular precursors will provide access to a wide range of other GNR shapes and widths and thus enable the engineering of electronic properties. For example, the $N = 7$ armchair GNR obtained from precursor **1** (Fig. 2) exhibits a bandgap of 1.6 eV (Supplementary Fig. 4), whereas the related $N = 9$ and $N = 11$ ribbons are predicted to exhibit much smaller bandgaps of about 0.7 eV and 0.2 eV, respectively (Supplementary Fig. 6)[2,6,28]. The chevron-like GNR consisting of alternating $N = 6$ and $N = 9$ segments (Fig. 3) exhibits the same bandgap of 1.6 eV (Supplementary Fig. 4) despite its different topology. However, its conduction bands are much less strongly dispersing, indicating a significant degree of charge carrier localization owing to the peculiar 'zigzag' shape of the ribbon (Supplementary Fig. 5). This suggests that the rational design of GNR width and shape (topology) allows not only for a detailed engineering of the bandgap, but also of the band curvature and thus the effective mass (mobility) of charge carriers.

Our bottom-up GNR fabrication process is not limited to Au(111) templates, with Ag(111) equally suitable for the fabrication of the two types of GNRs discussed above. This is illustrated by the sample in Fig. 4a, with the straight $N = 7$ GNRs and the chevron-type $N = 6/N = 9$ GNRs having been grown sequentially on a Ag(111) surface. Incidentally, a sample containing both GNRs is also obtained if both precursor monomers are deposited together on the substrate surface and the thermal activation sequence is then applied to the mixed sample. The intermolecular coupling reaction is thus highly selective: the design of the two monomers allows only homomolecular reactions, whereas heteromolecular coupling is sterically hindered.

But monomers can also be specifically designed for heteromolecular coupling. This is illustrated in Fig. 4b–d with the tri-halogen-functionalized monomer 1,3,5-tris(4′′-iodo-2′-biphenyl)benzene (monomer **3**), which has C_3 symmetry and provides no steric hindrance against radical addition to monomer **2** to yield the threefold GNR junction seen in the STM image in Fig. 4b. The strategy of using two different precursor monomers designed for facile heteromolecular coupling and cyclodehydrogenation should also enable the controlled growth of GNR heterojunctions. Our bottom-up GNR fabrication even holds promise for the growth of chemically doped GNRs from precursor monomers with phenyl rings substituted by heterocycles (with heteroatoms at positions that do not interfere with cyclodehydrogenation), leading to isostructural GNRs but with heteroatoms at strictly defined positions along the ribbon edges.

The present bottom-up route to atomically precise GNRs involves modest temperatures (<450 °C) compatible with current complementary metal–oxide–semiconductor (CMOS) technology, and all fabrication steps are performed *in situ* so that the intrinsic properties of the GNRs can be probed on clean and well-defined substrates. However, the technological use of this fabrication method faces some challenges, such as its extension to substrates that are technologically relevant while still being able to induce the dehalogenation, C–C coupling and cyclodehydrogenation steps. An alternative might be offered by the adaptation of transfer methods developed for epitaxial graphene[29,30], with preliminary results using a simple 'chip-to-chip press' method indicating that intact GNRs can be successfully transferred from gold films onto a SiO_2 substrate (Supplementary Fig. 7).

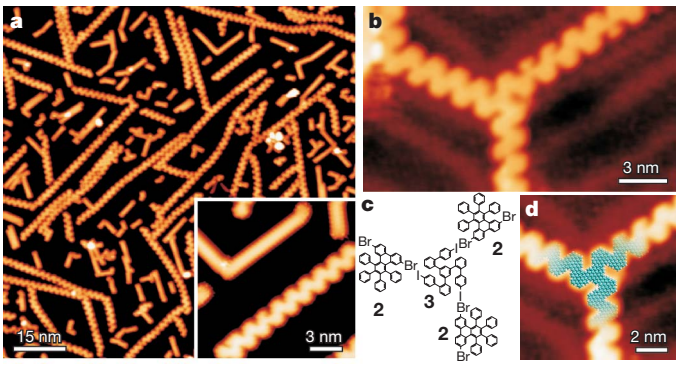

Figure 4 | Versatility of bottom-up GNR synthesis. a, STM image of coexisting straight $N = 7$ and chevron-type GNRs sequentially grown on Ag(111) ($T = 5$ K, $U = -2$ V, $I = 0.1$ nA). **b**, Threefold GNR junction obtained from a 1,3,5-tris(4′′-iodo-2′-biphenyl)benzene monomer **3** at the nodal point and monomer **2** for the ribbon arms: STM image on Au(111) ($T = 115$ K, $U = -2$ V, $I = 0.02$ nA). Monomers **2** and **3** were deposited simultaneously at 250 °C followed by annealing to 440 °C to induce cyclodehydrogentation. **c**, Schematic model of the junction fabrication process with components **3** and **2**. **d**, Model (blue, carbon; white, hydrogen) of the colligated and dehydrogenated molecules forming the threefold junction overlaid on the STM image from **b**.

METHODS SUMMARY

Preparation of GNRs. Au(111) and Ag(111) single crystals (Surface Preparation Laboratory, Netherlands) as well as 200 nm Au(111) thin films epitaxially grown on mica (Phasis, Switzerland) were used as substrates for GNR growth. Substrate surfaces were cleaned by repeated cycles of argon ion bombardment and annealing to 470 °C. Precursor monomers (for details on the synthesis, see the Supplementary Information) were deposited onto the clean substrate surfaces by sublimation from a sixfold evaporator (Knudsen-cell type) at rates of ~1 Å min^{-1}. Owing to a large distance between substrate and evaporator in our ultrahigh-vacuum set-up, only ~2% of the sublimated material reaches the sample. For the fabrication of straight $N = 7$ armchair GNRs, the substrate was maintained at 200 °C during monomer deposition to induce dehalogenation and radical addition. After deposition, the sample was post-annealed at 400 °C for 10 min to cyclodehydrogenate the polymers and form GNRs. For the chevron-type GNRs, the preparation process was identical, except that slightly higher substrate temperatures of 250 °C and 440 °C were used during monomer deposition and for post-annealing, respectively. In both cases, essentially all deposited monomers are transformed into the desired GNR structures.

STM characterization of GNRs. A variable-temperature STM and a low-temperature STM, both from Omicron Nanotechnology, were used to characterize the morphology of the GNR samples. Images were taken in the constant current mode under ultrahigh-vacuum conditions at sample temperatures of 298 K (room temperature), 115 K (liquid N_2 cooling) or 35 K (liquid He cooling) in the variable-temperature STM and 77 K or 5 K in the low-temperature STM.

Monomer synthesis, spectroscopic characterization, DFT calculations. Details regarding the synthesis of the precursor monomers, the Raman and XPS experiments, DFT calculations and STM simulations are given in the Supplementary Information.

Received 14 January; accepted 24 May 2010.

1. Wakabayashi, K. Electronic transport properties of nanographite ribbon junctions. *Phys. Rev. B* **64**, 125428 (2001).
2. Barone, V., Hod, O. & Scuseria, G. E. Electronic structure and stability of semiconducting graphene nanoribbons. *Nano Lett.* **6**, 2748–2754 (2006).
3. Son, Y. W., Cohen, M. L. & Louie, S. G. Half-metallic graphene nanoribbons. *Nature* **444**, 347–349 (2006).
4. Novoselov, K. S. *et al.* Electric field effect in atomically thin carbon films. *Science* **306**, 666–669 (2004).
5. Geim, A. K. Graphene: status and prospects. *Science* **324**, 1530–1534 (2009).
6. Yang, L., Park, C. H., Son, Y. W., Cohen, M. L. & Louie, S. G. Quasiparticle energies and band gaps in graphene nanoribbons. *Phys. Rev. Lett.* **99**, 186801 (2007).
7. Datta, S. S., Strachan, D. R., Khamis, S. M. & Johnson, A. T. C. Crystallographic etching of few-layer graphene. *Nano Lett.* **8**, 1912–1915 (2008).
8. Campos-Delgado, J. *et al.* Bulk production of a new form of sp(2) carbon: crystalline graphene nanoribbons. *Nano Lett.* **8**, 2773–2778 (2008).
9. Yang, X. Y. *et al.* Two-dimensional graphene nanoribbons. *J. Am. Chem. Soc.* **130**, 4216–4217 (2008).
10. Li, X. L., Wang, X. R., Zhang, L., Lee, S. W. & Dai, H. J. Chemically derived, ultrasmooth graphene nanoribbon semiconductors. *Science* **319**, 1229–1232 (2008).
11. Chen, Z. H., Lin, Y. M., Rooks, M. J. & Avouris, P. Graphene nano-ribbon electronics. *Physica E* **40**, 228–232 (2007).
12. Han, M. Y., Ozyilmaz, B., Zhang, Y. B. & Kim, P. Energy band-gap engineering of graphene nanoribbons. *Phys. Rev. Lett.* **98**, 206805 (2007).
13. Jiao, L. Y., Zhang, L., Wang, X. R., Diankov, G. & Dai, H. J. Narrow graphene nanoribbons from carbon nanotubes. *Nature* **458**, 877–880 (2009).

14. Kosynkin, D. V. *et al.* Longitudinal unzipping of carbon nanotubes to form graphene nanoribbons. *Nature* **458,** 872–875 (2009).
15. Elías, A. L. *et al.* Longitudinal cutting of pure and doped carbon nanotubes to form graphitic nanoribbons using metal clusters as nanoscalpels. *Nano Lett.* **10,** 366–372 (2009).
16. Jiao, L., Wang, X., Diankov, G., Wang, H. & Dai, H. Facile synthesis of high-quality graphene nanoribbons. *Nature Nanotechnol.* **5,** 321–325 (2010).
17. Grill, L. *et al.* Nano-architectures by covalent assembly of molecular building blocks. *Nature Nanotechnol.* **2,** 687–691 (2007).
18. Gourdon, A. On-surface covalent coupling in ultrahigh vacuum. *Angew. Chem. Int. Edn Engl.* **47,** 6950–6953 (2008).
19. Otero, G. *et al.* Fullerenes from aromatic precursors by surface-catalysed cyclodehydrogenation. *Nature* **454,** 865–868 (2008).
20. Rim, K. T. *et al.* Forming aromatic hemispheres on transition-metal surfaces. *Angew. Chem. Int. Edn Engl.* **46,** 7891–7895 (2007).
21. Huang, L., Lai, Y. C., Ferry, D. K., Akis, R. & Goodnick, S. M. Transmission and scarring in graphene quantum dots. *J. Phys. Condens. Matter* **21,** 344203 (2009).
22. Sevincli, H., Topsakal, M. & Ciraci, S. Superlattice structures of graphene-based armchair nanoribbons. *Phys. Rev. B* **78,** 245402 (2008).
23. Malard, L. M., Pimenta, M. A., Dresselhaus, G. & Dresselhaus, M. S. Raman spectroscopy in graphene. *Phys. Rep.* **473,** 51–87 (2009).
24. Vandescuren, M., Hermet, P., Meunier, V., Henrard, L. & Lambin, P. Theoretical study of the vibrational edge modes in graphene nanoribbons. *Phys. Rev. B* **78,** 195401 (2008).
25. Classen, T. *et al.* Templated growth of metal-organic coordination chains at surfaces. *Angew. Chem. Int. Edn Engl.* **44,** 6142–6145 (2005).
26. Canas-Ventura, M. E. *et al.* Self-assembly of periodic bicomponent wires and ribbons. *Angew. Chem. Int. Edn Engl.* **46,** 1814–1818 (2007).
27. Briggs, D. & Beamson, G. *High Resolution XPS of Organic Polymers: The Scienta ESCA300 Database* Appendix I (John Wiley & Sons, 1992).
28. Son, Y. W., Cohen, M. L. & Louie, S. G. Energy gaps in graphene nanoribbons. *Phys. Rev. Lett.* **97,** 216803 (2006).
29. Lee, Y. *et al.* Wafer-scale synthesis and transfer of graphene films. *Nano Lett.* **10,** 490–493 (2010).
30. Caldwell, J. D. *et al.* Technique for the dry transfer of epitaxial graphene onto arbitrary substrates. *ACS Nano* **4,** 1108–1114 (2010).

Supplementary Information is linked to the online version of the paper at www.nature.com/nature.

Acknowledgements This work was supported by the Swiss National Science Foundation and the NCCR Nanoscale Science. R.F. and P.R. thank O. Gröning and P. Gröning for stimulating discussions and continued support. A.P.S. acknowledges discussions with F. Mauri and M. Lazzeri. The Mainz group acknowledges financial support from the Max Planck Society through the program ENERCHEM, the German Science Foundation (Korean-German IRTG), the DFG Priority Program SPP 1355 and DFG MU 334/32-1.

Author Contributions P.R, R.F., X.F. and K.M. conceived the experiments. M.S. synthesized the molecular precursors. J.C., R.J., M.B. and P.R. performed the growth and scanning probe experiments. T.B. and M.M. did the spectroscopic analysis. S.B. and A.P.S. performed the simulations. J.C., P.R. and R.F. prepared the figures. P.R., J.C. and R.F. wrote the paper. All authors discussed the results and implications and commented on the manuscript at all stages.

Author Information Reprints and permissions information is available at www.nature.com/reprints. The authors declare no competing financial interests. Readers are welcome to comment on the online version of this article at www.nature.com/nature. Correspondence and requests for materials should be addressed to R.F. (roman.fasel@empa.ch) or K.M. (muellen@mpip-mainz.mpg.de).